Journal of Solid State Chemistry

Volume 198, Pages 1-548 (February 2013)

Original Research Article
Pages 10-17
J.M. Allred, R.J. Cava

Highlights

► Crystal structures of the metallic forms of V_8O1_5 and V9O17. ► General trends across the V_n O_2n-1 allow designation of two chain types in all phases. ► Triclinic *b* lattice parameter varies anomalously with *n*, in V_n O_2n-1. ► Trend in *b* matches the metal to insulator transition temperature trend.

Syntheses, characterization and magnetic properties of two novel inorganic-organic tungstoferrites, $[Fe^{III}_4(H_2O)_2(B\text{-}\alpha\text{-}Fe^{III}W_9O3_4)2]^{10}$-

Original Research Article
Pages 18-23
Dongdi Zhang, Chunzhang Wang, Suzhi Li, Jiangping Liu, Pengtao Ma, Jingping Wang, Jingyang Niu

Highlights

► **1** represents the first example of 1D chain-like $\{Fe_4(FeW_9)_2\}$ tungstoferrite. ► Two $[B\text{-}a\text{-}Fe^{III}W_9O34]^{11-}$ units linked via a rhomb-like tetranuclear iron cluster. ► Adjacent $\{Fe_4(FeW_9)_2\}$ are interconnected by unusual WDODFe bridges. ► Antiferromagnetic exchange interactions are dominant in the $\{Fe_6O_{22}\}$ cluster.

Crystal structures and high-temperature phase-transitions in $SrNdMRuO_6$ (*M*=Zn,Co,Mg,Ni) new double perovskites studied by symmetry-mode analysis

Original Research Article
Pages 24-38
E. Iturbe-Zabalo, J.M. Igartua, A. Faik, A. Larrañaga, M. Hoelzel, G.J. Cuello

► Structural study of four ruthenate double perovskites. ► Room-temperature structural determination using symmetry-mode procedure. ► Determination of temperature induced structural phase-transitions. ► Symmetry adapted-mode analysis.

Novel alkaline earth copper germanates with ferro and antiferromagnetic *S=1/2* chains

Original Research Article
Pages 39-44
Paula Brandão, Mario S. Reis, Zheng Gai, António M. dos Santos

Highlights

► The structure of two new chain containing copper germinates is reported. ► The calcium compound CaCuGcO, ■ H_20contains corner sharing square planes. ► The barium compound $BaCu_2Ge_3O_9$, displays edge sharing octahedra. ► Susceptibility data show that the Ca compound is a one-dimensional antiferromagnet while Ba is a weak ferromagnet

Synthesis of lithium cobalt oxide by single-step soft hydrothermal method

Original Research Article
Pages 45-49
Kiran Kumar Bokinala, M. Pollet, A. Artemenko, M. Miclau, I Grozescu

Graphical abstract

Highlights

► An optimized soft hydrothermal method for a fast synthesis of high purity $LiCoO_2$ compound is reported. ► Both lamellar and cuboctahedral particles could be stabilized. ► Secondary phases content is lower than 0.1%. ► Close to surface defects were evidenced using EMR.

Ternary aluminides $R_0.67Ni_2Al_6$ *(R=Sc,* Y, Gd-Lu) with partly disordered structures

Original Research Article
Pages 50-56

Oksana Matselko, Svitlana Pukas, Yuriy Lutsyshyn, Roman Gladyshevskii, Dariusz Kaczorowski

Graphical abstract

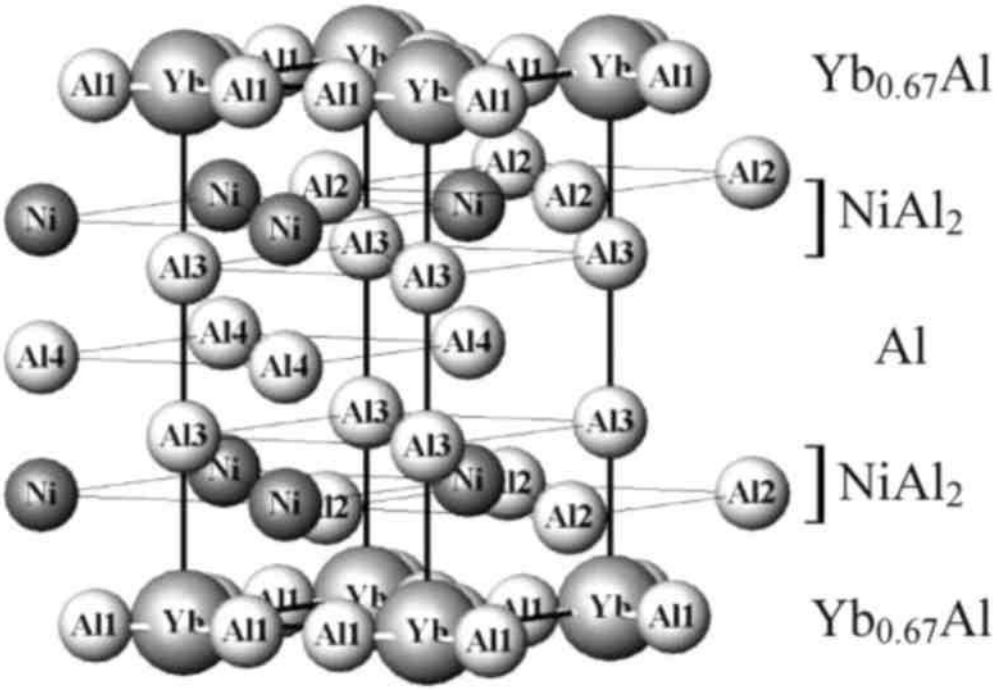

Highlights

► The aluminides $R_0.67Ni_2Al_6$ *(R=Sc, Y,* Gd-Lu) adopt a partly disordered structure. ► The structure is characterized by R_2Al_3 layers with two *R* atoms for one Al_3 triangle. ► The compounds with *R*=Tb, Er, Tm are paramagnets at rt and order magnetically at lt. ► The Yb-compound exhibits a magnetically ordered Kondo lattice with strong CEF effect.

Synthesis and single crystal structure refinement of the one-layer hydrate of sodium brittle mica

Original Research Article
Pages 57-64
Hussein Kalo, Wolfgang Milius, Michael Bräu, Josef Breu

Graphical abstract

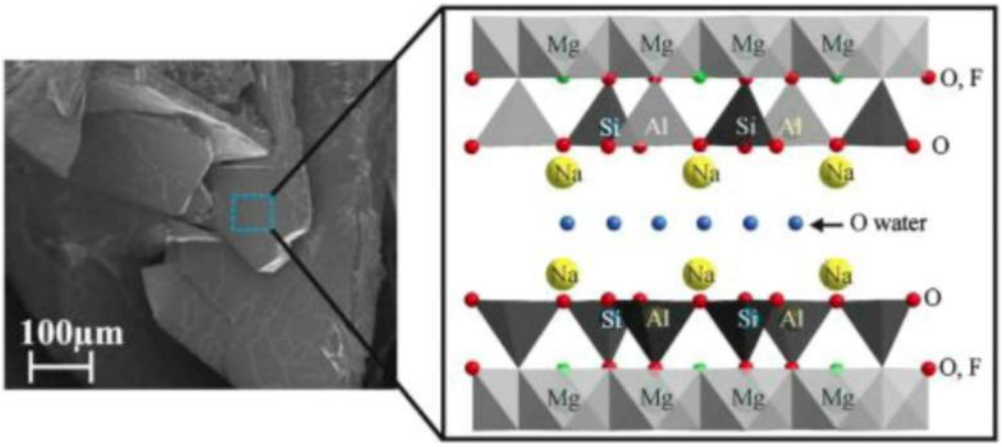

Highlights

► Melt synthesis yielded coarse grained sodium brittle mica which showed little disorder. ► Sodium brittle mica hydrated completely to the state of one-layer hydrate. ► Structure of one-layer hydrate of sodium brittle mica could therefore be determined and refined. ► Arrangement of upper and lower tetrahedral sheet encompassing interlayer cation were clarified.

The defect chemistry of nitrogen in oxides: A review of experimental and theoretical studies

Original Research Article
Pages 65-76
Jonathan M. Polfus, Truls Norby, Reidar Haugsrud

Highlights

► Experimental and theoretical investigations of the nitrogen and hydrogen related defect chemistry of wide band gap oxides is reviewed. ► The interaction between nitrogen dopants and protons is important and emphasized. ► Diffusion and photocatalytic properties of N-doped oxides are discussed.

Electronic structure and optical properties of the nonlinear optical crystal $Pb_4O(BO_3)_2$ by first-principles calculations

Original Research Article
Pages 77-80
Zhihua Yang, Shilie Pan, Hongwei Yu, Ming-Hsien Lee

Highlights

► Lone pair effect on Pb^{2+} and delocalization ,rorbital in BO_3 group is studied. ► The combination of PbO*n* (*n*=3,4,5) and BO_3 group makes $Pb_4O(BO_3)_2$ a large SHG effect. ► $Pb_4O(BO_3)_2$ is a direct gap material with the gap 2.608 eV by the *ab initio* method. ► The calculated birefringence is about 0.039-0.061 with the wavelength of about 375 nm. ► The second-order susceptibility $d_24=3.5d_{36}$ (KDP) in accordance with the experimental result.

Synthesis, structural characterization and optical properties of new compounds: Centrosymmetric Ba_2GaMQ_5 (M=Sb,Bi; Q=Se,Te), $Ba_2InSbTe_5$ and noncentrosymmetric $Ba_2InSbSe_5$

Original Research Article
Pages 81-86
Wenyu Hao, Dajiang Mei, Wenlong Yin, Kai Feng, Jiyong Yao, Yicheng Wu

Highlights

► Ba_2GaMQ_5 (M=Sb,Bi; Q=Se,Te) and Ba_2InSbQ_5 (Q=Se,Te) have been synthesized. ► The structures contain infinite ^MM'Q^''(M′=Ga,In) anionic chains. ► The chains are built by distorted MQ_6 (M=Sb,Bi) octahedra and M′Q_4 (M′=Ga,In) tetrahedra. ► $Ba_2InSbSe_5$ exhibits a weak powder second harmonic generation signal.

A series of novel gallium and indium borates constructed from $[B_5O_8(OH)_2]^{3-}$ clusters and metal complex linkers

Original Research Article
Pages 87-92
Lin Cheng, Guo-Yu Yang

Highlights

► Four new Ga/In borates have been hydrothermally made. ► The helical/ribbon-like chains made of $B_5O_8(OH)_2^{3+}$ clusters and Ga-/In-complex linkers. ► The chains form novel 3-D supermolecule framework via H-bonds.

Narrow spectral emission $CaMoO_4$: Eu^{3+}, Dy^{3+}, Tb^{3+} phosphor crystals for white light emitting diodes

Original Research Article
Pages 93-100

A. Khanna, PS. Dutta

Highlights

► $CaMoO_4$: Ln^{3+} (Ln=Eu^{3+}, Dy^{3+}, Tb^{3+}) phosphor crystals were successfully grown using high temperature flux (solutions) containing molybdenum (VI) oxide or lithium chloride. ► Narrow spectral emission at 615 nm, 575 nm and 550 nm, respectively, was observed from $CaMoO_4$: Ln^{3+} (Ln=Eu^{3+}, Dy^{3+}, Tb^{3+}) phosphor crystals. ► The optimized doping concentrations of Eu^{3+}, Dy^{3+}, Tb^{3+} in $CaMoO_4$ for highest emission intensity were determined to be 12%, 2% and 5%, respectively. ► The $CaMoO_4$: Ln^{3+} (Ln=Eu^{3+}, Dy^{3+}, Tb^{3+}) phosphor crystals grown with molybdenum (VI) oxide flux exhibited 50% higher emission intensity compared to the crystals grown with lithium chloride flux and the powders synthesized by solid-state reaction.

Lattice crossover and phase transitions in $NdAlO_3$-$GdAlO_3$ system

Original Research Article
Pages 101-107
L. Vasylechko, H. Shmanko, N. Ohon, Yu. Prots, S. Hoffmann, S. Ubizskii

Highlights

► Two kinds of solid solutions $Nd1-_xGd_xAlO_3$ were found in the $NdAlO_3$-$GdAlO_3$ system. ► Morphotropic transition between both perovskite phases occurs at $x\approx0.15$. ► Lattice parameter crossover was found in orthorhombic solid solution. ► Temperature driven first-order phase transition *Pbnm*↔*R* **3** *c* was found in $Nd1-_xGd_xAlO_3$. ► Phase diagram of the pseudo-binary system $NdAlO_3$-$GdAlO_3$ has been constructed.

Effects of competing magnetic interactions on the electronic transport properties of $CuCrSe_2$

Original Research Article
Pages 108-113
Girish C. Tewari, Maarit Karppinen, Ashok K. Rastogi

► Layered $CuCrSe_2$ can be synthesized in both fully and partially cation-ordered forms. ► Contrary to previously believed insulating nature the cation-ordered phase is metallic. ► Magnetic property of $CuCrSe_2$ is somewhat different from that of $CuCrS_2$. ► Magnetization and heat capacity data suggest complex short-range ordering for $CuCrSe_2$.

Magnetic properties of mesoporous cobalt-silica-alumina ternary mixed oxides

Original Research Article
Pages 114-119
Nabanita Pal, Md. Motin Seikh, Asim Bhaumik

Graphical Abstract

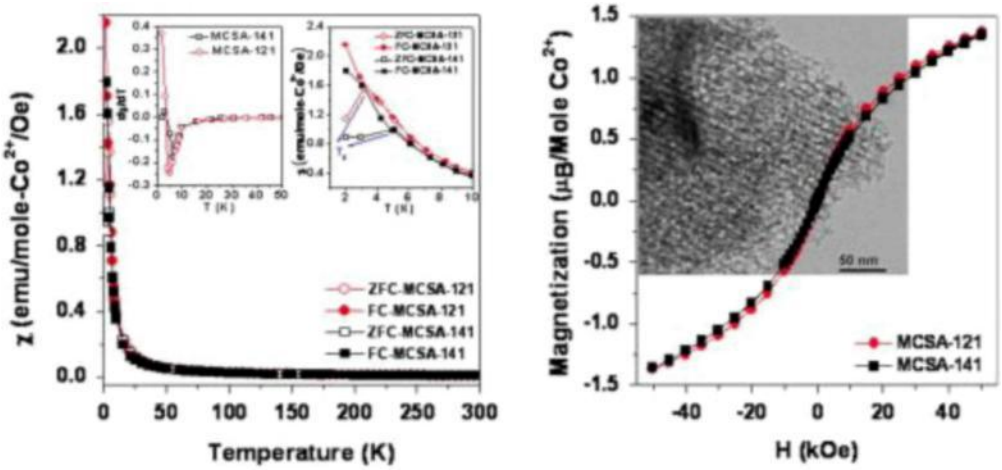

Highlights

► Mesoporous cobalt-silica-alumina ternary mixed oxides. ► High surface area and mesoporosity in magnetic materials. ► Ferromagnetic correlation at elevated temperature. ► Low temperature paramagnetic to ferrimagnetic transition.

First-principles study for ferromagnetism of Cu-doped ZnO with carrier doping

Original Research Article
Pages 120-124
Byung-Sub Kang, Kyeong-Sup Kim, Seong-Cho Yu, Heejoon Chae

Graphical abstract

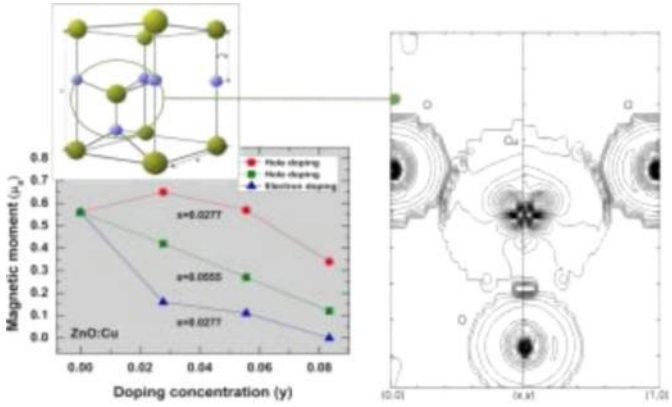

Highlights

► The ferromagnetism of Cu-doped ZnO is controllable by N or F carrier density. ► The Cu magnetic moment in low Cu concentration is increased by hole doping. ► The N 2*p* states hybridize well with the Cu 3*d* states instead of the O 2*p* states. ► For (Cu,F)-codoped ZnO, the Cu 3*d* band is narrower than that for (Cu,N)-codoped ZnO.

Thermoelectric properties of fine-grained FeVSb half-Heusler alloys tuned to *p*-type by substituting vanadium with titanium

Original Research Article
Pages 125-130
Minmin Zou, Jing-Feng Li, Takuji Kita

Graphical abstract

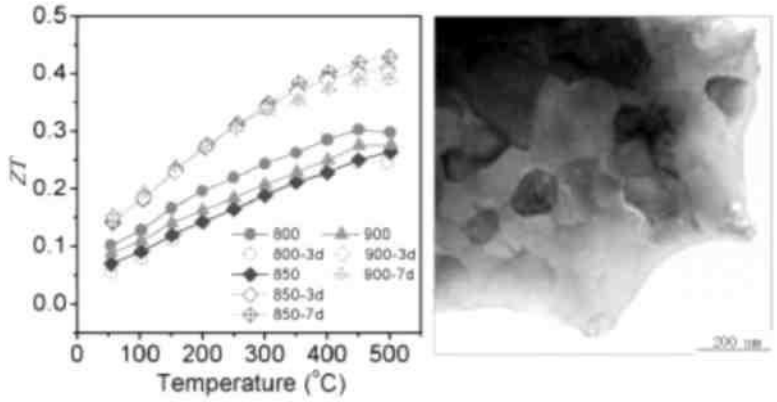

Highlights

► Ti-doped FeVSb half-Heusler alloys were synthesized by combining MA and SPS. ► Substituting V with Ti changes the electrical behavior from *n*-type to *p*-type. ► Thermoelectric

properties are improved by optimizing sintering temperature. ► Thermoelectric properties are further improved by applying annealing treatment. ► A high *ZT* value of 0.43 is obtained at 500 °C for *p*-type Ti-doped FeVSb alloys.

Synthesis and characterization of hybrid nanostructures produced in the presence of the titanium dioxide and bioactive organic substances by hydrothermal method

Original Research Article
Pages 131-137
Tatyana Zima, Natalya Baklanova, Ivan Bataev

Graphical abstract

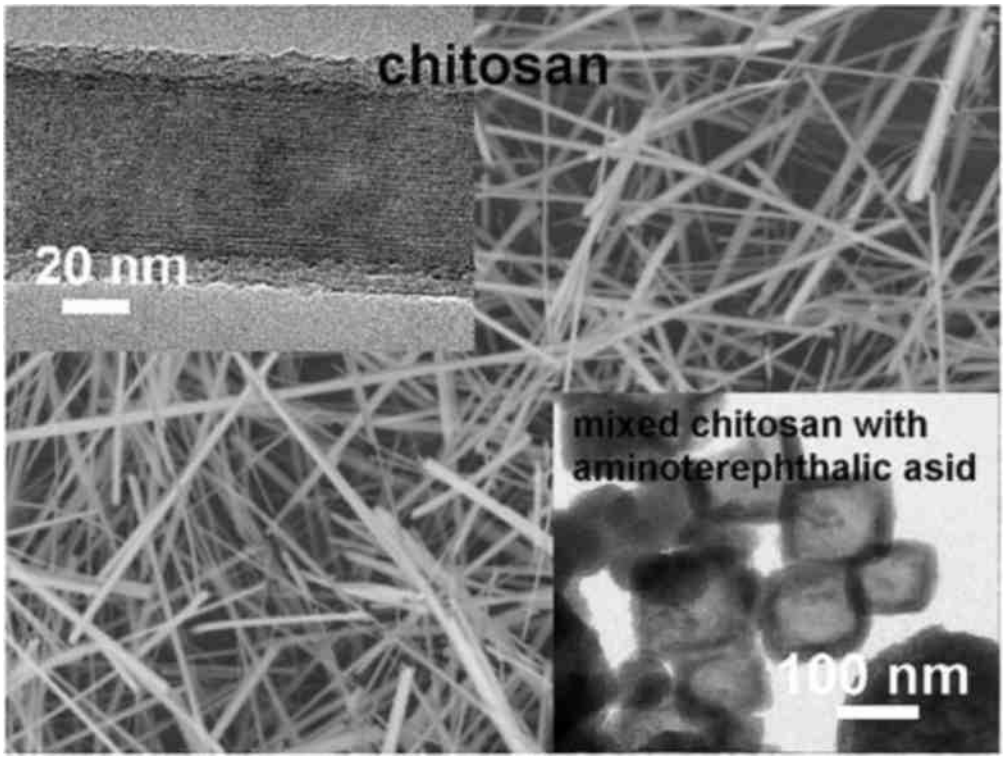

Highlights

► Various shapes of TiO_2 based structures can be produced in the presence of organic. ► An addition of chitosan results in the formation of the elongated nanostructures. ► These structures have multilayered morphology and increased distance between layers. ► Different agglomerates are formed when chitosan and aminoterephthalic acid are mixed.

Framework-incorporated Mn and Co analcime zeolites: Synthesis and characterization

Original Research Article
Pages 138-142
Seyed Naser Azizi, Salma Ehsani Tilami

Graphical abstract

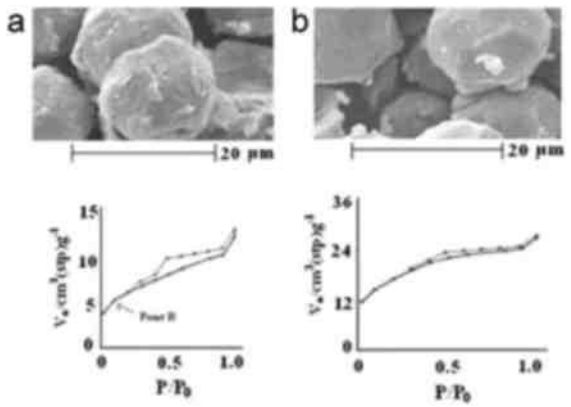

Highlights

► Synthesis of Co and Mn modified analcime for the first time. ► Framework-incorporation of Co and Mn using the same silicate gel composition. ► Applying several techniques to provide proofs for the characterization.

Design and construction of porous metal-organic frameworks based on flexible BPH pillars

Original Research Article
Pages 143-148
Xiang-Rong Hao, Guang-sheng Yang, Kui-Zhan Shao, Zhong-Min Su, Gang Yuan, Xin-Long Wang

Graphical abstract

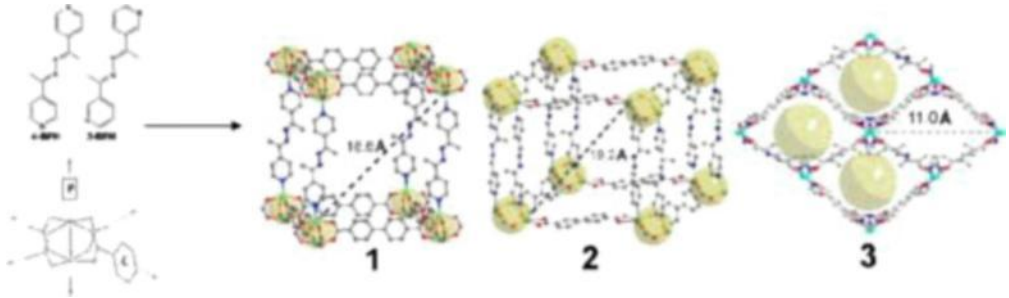

Highlights

► Frameworks **1** and **2** have MOF-5 like motif. ► The cube-like cages in **1** and **2** are quite large, comparable to the IRMOF-10. ► Framework **1** is “single-pillared” mode while **2** is “double-pillared” mode. ► PXRD and gas adsorption analysis show that **3** is a dynamic porous framework.

Phase relations and structural features in the system Ni-Zn-B

Original Research Article
Pages 150-161
Z. Malik, A. Grytsiv, P. Rogl, G. Giester, J. Bursik

Graphical abstract

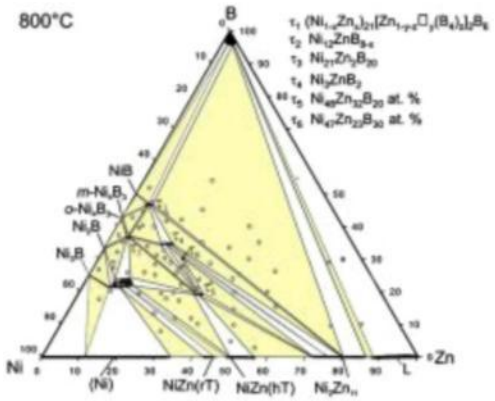

Highlights

► Phase relations were determined for the system Ni-Zn-B at 800 °C. ► Existence of six ternary compounds (T_1–T_6) has been confirmed at 800 °C. ► Homogeneity range for ***n*** with respect to Ni/Zn and Zn/B at 800 °C has been determined. ► The crystal structures of T_5-$Ni_48Zn_32B_20$ from TEM (*oI*, *a*=1.6(2) nm, *b*=0.63(7) nm, and *c*=0.27(0) nm). ► Precise data on T_1-$(Ni1-_xZn_x)_21[Zn1-_y-_z\wedge(B_4)_z]2B_6$ ($0.07\leq x\leq 0.11$, $0.07\leq y\leq 0.53$, $0\leq z\leq 0.3$), *o*-Ni_4B_3-$_x$ and *m*-Ni_4B_3 have been presented.

Three tetranuclear copper(II) cluster-based complexes constructed from 4-amino-1,2,4-triazole and different aromatic carboxylates: Assembly, structures, electrochemical and magnetic properties

Original Research Article
Pages 162-168

Xiu-Li Wang, Wei Zhao, Ju-Wen Zhang, Qi-Lin Lu

Highlights

► Three new tetranuclear copper(II) cluster-based complexes have been obtained. ► The atrz conduces to the construction of tetranuclear copper(II) clusters. ► Carboxylates show important effect on the structures of title complexes. ► Magnetic properties and electrochemical behaviors have been reported.

Synthesis of $Sr_0.9K0.1FeO_3$-δ electrocatalysts by mechanical activation

Original Research Article
Pages 169-175
J.F. Monteiro, J.C. Waerenborgh, A.V. Kovalevsky, A.A. Yaremchenko, J.R. Frade

graphical abstract

XRD patterns of $Sr_0.9K0.1FeO_3$-δ powders, as-prepared and after annealing at different temperatures.

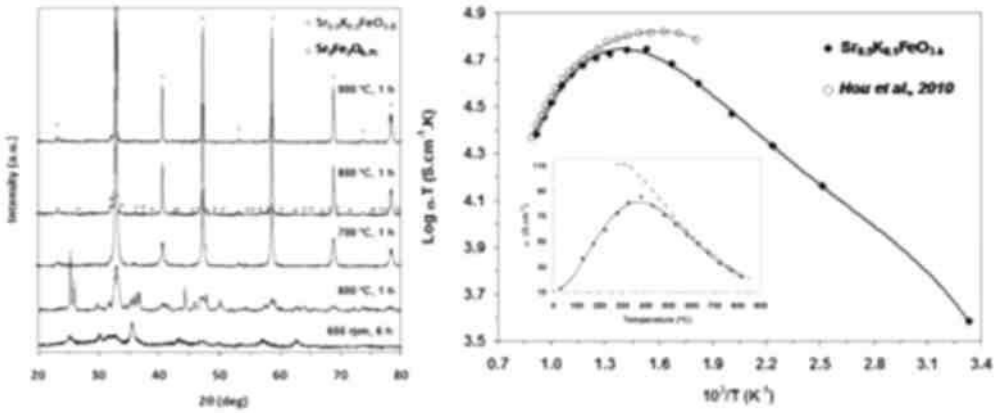

Highlights

► $Sr_0.9K0.1FeO_3$-δ was successfully obtained by mechanical activation of oxide precursors. ► Synthesis temperature is significantly lower when compared to a conventional solid-state route. ► Oxygen nonstoichiometry of annealed samples at 900-1100 °C vary in the range *8=030*-0.32. ► $Sr_0.9K0.1FeO_3$-δ shows metal and semiconductor behaviour above and below 400 °C, respectively.

Magnetic properties and structural transitions of fluorite-related rare earth osmates Ln_3OsO_7 *(Ln=Pr,* Tb)

Original Research Article
Pages 176-185
Yukio Hinatsu, Yoshihiro Doi

Highlights

► Ternary rare-earth osmates Ln_3OsO_7 (*Ln*=Pr, Tb) with an ordered defect-fluorite structure have been prepared. ► Both of these compounds undergo a structural phase transition at 130 K (*Ln*=Pr) and 580 K (*Ln*=Tb). ► These compounds show complex magnetic behavior at low temperatures due to magnetic ordering of *Ln* and Os.

Structure and magnetic properties of $Ba_5Ce_{1.25}Mn_{3.75}O_{15}$, a new 10*H*-polytype in the Ba–Ce–Mn–O system

Original Research Article
Pages 186-191
Mario A. Macías, Olivier Mentré, Silviu Colis, Gabriel J. Cuello, Gilles H. Gauthier

Graphical abstract

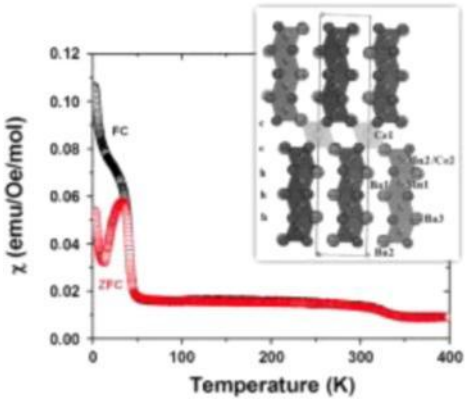

Highlights

► $Ba_5Ce1._{25}Mn_3.75O1_5$, a new 10*H* polytype, has been prepared in the Ba-Ce-Mn–O system. ► The compound crystallizes in the $P6_3/mmc$ space group with $(cchhh)_2$ stacking sequence. ►

[Ce_0.25Mn_3.75$O1_5$] tetramers are separated by [CeO_6] octahedra in the structure. ► Instead of robust AFM ordering, a metamagnetic-like transition is found around 50 K.

Preparation and photocatalytic activity for water splitting of Pt-$Na_2Ta_2O_6$ nanotube arrays

Original Research Article
Pages 192-196
Jing Liu, Jiawen Liu, Zhonghua Li

Highlights

► Novel $Na_2Ta_2O_6$ nanotube array films with pyrochlore structure were synthesized. ► $Na_2Ta_2O_6$ nanotube arrays are active for H_2 evolution from aqueous CH_3OH solution. ► The effect of hydrothermal conditions on photocatalytic activity was investigated. ► Pt loading can improve the photocatalytic activities of $Na_2Ta_2O_6$ nanotube arrays. ► Photocatalytic mechanism is proposed based on the experimental results.

Influences of alcoholic solvents on spray pyrolysis deposition of TiO_2 blocking layer films for solid-state dye-sensitized solar cells

Original Research Article
Pages 197-202
Changyun Jiang, Wei Lin Koh, Man Yin Leung, Wei Hong, Yuning Li, Jie Zhang

Highlights

► Solvent influences morphology of spray pyrolysis deposited TiO_2 blocking layer. ► Ethanol reacts with TPA, resulting poor quality of blocking layer. ► Isopropanol is better than ethanol for obtaining smooth blocking layer. ► SDSC with blocking layer made with isopropanol showed better performance.

The synthesis and characterisation of $LaCa_2Fe_2GaO_8$

Original Research Article
Pages 203-209
Kun Luo, Michael A. Hayward

► $LaCa_2Fe_2GaO_8$ exhibits a novel anion-vacancy ordered triple-layer structure type. ► New structure variant rationalised on the basis of strucutral parameters. ► Multiple magnetic transitions: paramagnetic-two-dimensional-three-dimensional.

Mixed metallic Ba(Co,Mn)X_0.2-$_x$ O $_{3-й}$ *(X=F,* Cl) hexagonal perovskites

Original Research Article
Pages 210-217
Mihaela Iorgulescu, Pascal Roussel, Nathalie Tancret, Nicolas Renaut, Nicolas Tiercelin, Olivier Mentré

Graphical abstract

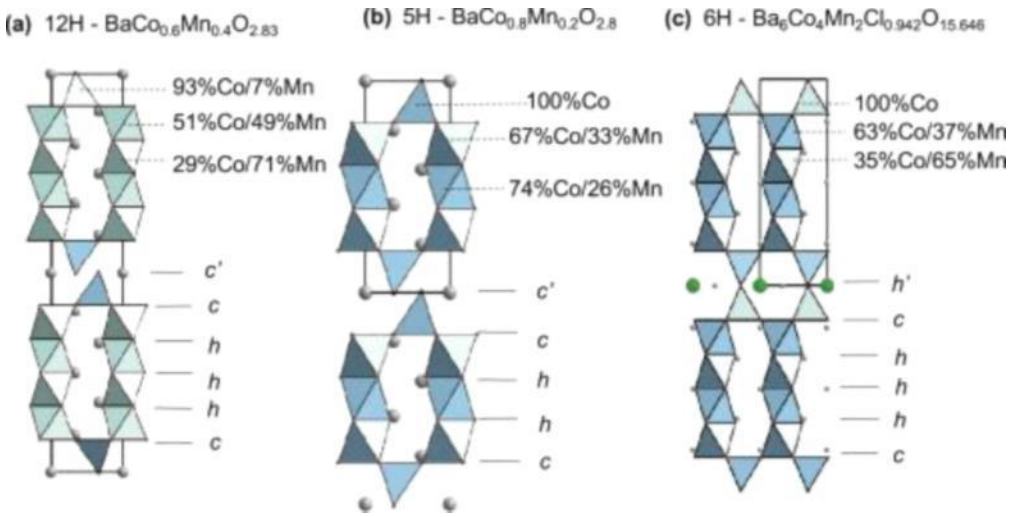

Highlights

► The incorporation of Mn in $BaCoX_{0.2-x}O_{3-}$ *(X=F,Cl)* hexagonal perovskites stabilizes the 6H-form. ► It contains tetrameric $(Co,Mn)_4O1_5$ face sharing linear chains. ► The preference for such chains better than trimeric ones is due to the Manganese oxidizing effect. ► A particular Mn/Co distribution was evidenced. ► Transport and magnetic properties drastically change during the Mn incorporation.

Photophysical properties of donor-∏-acceptor azoic chromophores adsorbed and intercalated into MgDAlDLDH

Original Research Article
Pages 218-223
Lei Li, Pengfei Liu, Li Zhang, Dazhou Chen

Graphical abstract

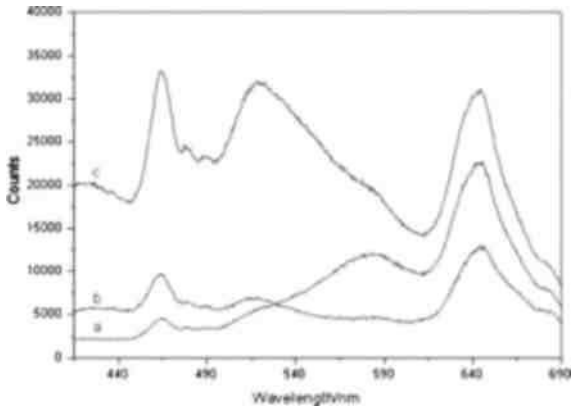

Highlights

► EO and AS are intercalated into LDHs or adsorbed on the external surface of LDHs. ► The host-guest interactions modulate photophysical properties of the guest. ► The guests having higher molecular dipole moments can enhance the blue emission.

Intercalation of organic molecules into SnS_2 single crystals

Original Research Article
Pages 224-230
ML. Toh, K.J. Tan, F.X. Wei, K.K. Zhang, H. Jiang, C. Kloc

► Organic molecules intercalated inhomogenously between covalently bonded SnS_2 layers. ► Ethylenediamine (en) intercalate directly into SnS_2. ► Phenylenediamine (PPD) and naphthalenediamine (NDA) can be intercalated into SnS_2 secondary. ► In a secondary

intercalation the bonds between layers are weakened by direct intercalation of (en). ► The optical band gap of SnS_2 is reduced due to intercalation.

Carbon supported tin-based nanocomposites as anodes for Li-ion batteries

Original Research Article
Pages 231-237
Xiangyang Zhou, Youlan Zou, Juan Yang

Graphical abstract

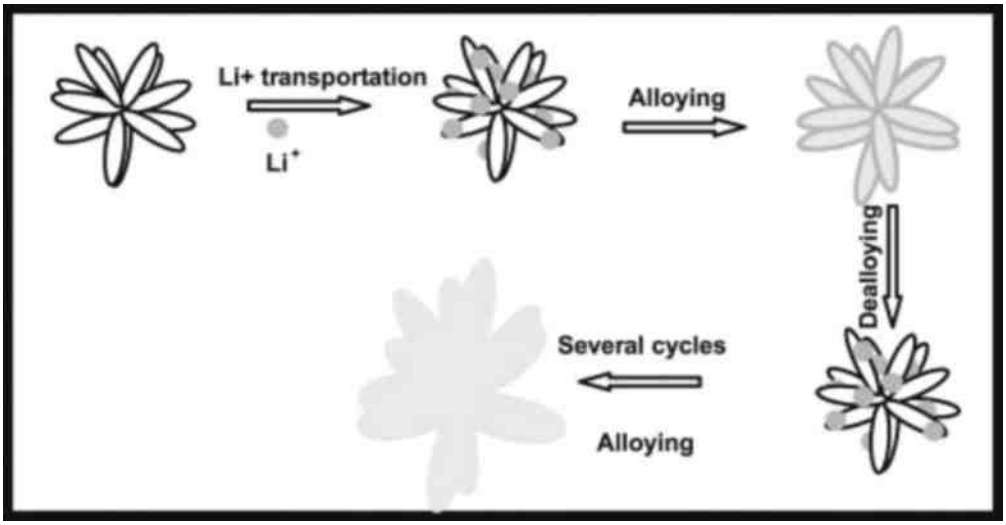

Highlights

► Carbon supported SnO_2 (Sn)/C composites have been synthesized. ► Temperature control affects the physical and electrochemical performance. ► Clusters of chrysanthemum-like microstructures were observed. ► Intervals exist between SnO_2 layers. ► Integrity structure of SnO_2/C composites was preserved.

Low temperature synthesis of τ-zirconium hydrogenophosphate [τ-$Zr(HPO_4)_2$] and a new sodic form obtained by ion exchange

Original Research Article
Pages 238-245
Suilma M. Fernández-Valverde, Aída Contreras-Ramírez, Eduardo Ordóñez-Regil, M. Eufemia Fernández-García, Mario Pérez-Álvarez

Graphical abstract

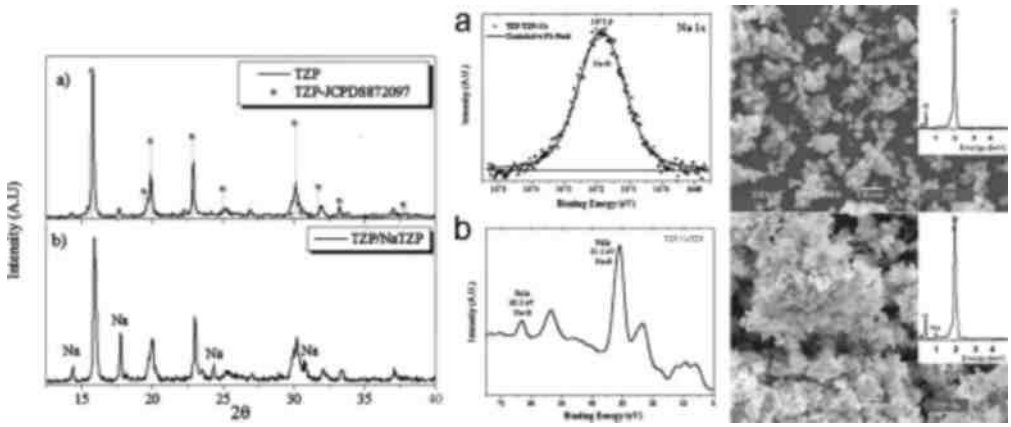

Highlights

► New method for the syntheses of 3-D τ-zirconium hydrogenophosphate (TZP). ► A sodic form of the TZP was obtained by the immersion of TZP in a sodium hydroxide. ► The sodium compound is only formed on the TZP surface.

Synthesis and characterization of oxyanion (phosphate, sulphate) doped $Ba_2Sc_{2-3},Ga\ O_5$

Original Research Article
Pages 247-252
AD. Smith, J.F. Shin, P.R. Slater

Highlights

► The successful synthesis of phosphate and sulphate doped $Ba_2Sc_{2-x}Ga_xO_5$ perovskites. ► The demonstration of significant oxide ion and proton conduction in these perovskites. ► The demonstration of improved CO_2 stability with increasing Ga content.

Cobalt–iron red–ox behavior in nanostructured $La_{0.4}Sr_{0.6}Co_{0.8}Fe_{0.2}O_{3-\delta}$ cathodes

Original Research Article
Pages 253-261
Analía L. Soldati, Laura Baqué, Federico Napolitano, Adriana Serquis

Graphical abstract

Highlights

► Red-ox treatments in LSCF nano-particles cause a reversible reaction. ► XPD analyses show that a new "reduced" phase coexist with the oxidize one. ► The B-site formal oxidation state decreases and the ***δ*** increases upon reduction. ► Fe remains in a higher valence (closer to 4+) than Co (close to 3+). ► The behavior seems to be independent of the synthesis method used.

Synthesis, structural and magnetic characterisation of the fully fluorinated compound 6H-$BaFeO_2F$

Original Research Article
Pages 262-269
Oliver Clemens, Adrian J. Wright, Frank J. Berry, Ronald I. Smith, Peter R. Slater

Highlights

► The crystal structure of the hexagonal perovskite phase 6H-$BaFeO_2F$. ► H-$BaFeO_2F$ and 6H-$BaFeO_{3-d}F_y$ were prepared via low temperature fluorination using PVDF. ► A structural investigation of the compounds $BaFeO_2F$ is presented in detail. ► This analysis suggests differences for the local coordination of O^2 and F anions. ► H-$BaFeO_2F$ shows antiferromagnetic ordering at 300 K. ► The magnetic moments align parallel to the *a*-axis.

Uranium diphosphonates templated by interlayer organic amines

Original Research Article
Pages 270-278
Anna-Gay D. Nelson, Evgeny V. Alekseev, Thomas E. Albrecht-Schmitt, Rodney C. Ewing

Highlights

► Organic amines act both as charge-balancing and as structure-directing agents. ► Extensive hydrogen bonding interactions with solvent water molecules and amines. ► Altering the organic amine (size or flexibility) affects structure formation.

A series of 2D metal-quinolone complexes: Syntheses, structures, and physical properties

Original Research Article
Pages 279-288
Jiang-Hong He, Dong-Rong Xiao, Hai-Yan Chen, Dian-Zhen Sun, Shi-Wei Yan, Xin Wang, Zhong-Li Ye, Qun-Li Luo, En-Bo Wang

Highlights

►Compounds **1**-**3** consist of novel 2D arm-shaped layers based on the 1D $\{M(COO)\}_n^{n+}$ chains. ► Compounds **4** and **5** are two novel 2D layers based on tetranuclear Mn or Co clusters with **kgd** topology. ► Compound **6** is the first example of metal-quinolone complexes with 2D bilayer structure. ► Compounds **1**-**6** represent six unusual examples of 2D metal-quinolone complexes.

Synthesis, structure and characterization of two new copper(I)-thioarsenates (III) constructed by the $[AsS_3]^{3-}$ and CuS_x units

Original Research Article
Pages 289-294
Hua-Gang Yao, Min Ji, Shou-Hua Ji, Yong-Lin An

Highlights

► We obtained two new copper(I)-thioarsenate(III), $CsCu_2AsS_3$ and KCu_4AsS_4. ► Both compounds possess noncondensed $[AsS_3]^{3-}$ unit and represent new structure types. ► The

optical band gaps of the two compounds are 2.3 eV and 1.8 eV, respectively.

Six novel transition-metal phosphite compounds, with structure related to yavapaiite: Crystal structures and magnetic and thermal properties of $A^{I}[M^{III}(HPO_3)_2]$ (A=K, NH_4, Rb and M=V, Fe)

Original Research Article
Pages 295-302
Farida Hamchaoui, Véronique Alonzo, Diego Venegas-Yazigi, Houria Rebbah, Eric Le Fur

Highlights

► A new family of transition metal phosphites has been prepared. ► The structure of these compounds is related to layered minerals like Yavapaiite. ► Antiferromagnetic coupling is evidenced suggesting possible magnetic frustration. ► Thermal studies show, in general, oxidation of phosphites into pyrophosphates.

Preparation of anionic clay–birnessite manganese oxide composites by interlayer oxidation of oxalate ions by permanganate

Original Research Article
Pages 303-307
James Arulraj, Michael Rajamathi

► Anionic and cationic layered solid composites prepared. ► Ni-Zn hydroxy oxalate reacted with $KMnO_4$ to deposit MnO_2 in the interlayer. ► Birnessite layers coexist with anionic clay layers in the composites. ► Birnessite/anionic clay ratio controlled by amount of $KMnO_4$ used and reaction time

Factors governing Yb magnetism in $Yb_{0.95}PtIn_2$ and other $MgCuAl_2$-type structures

Original Research Article
Pages 308-315
Andrew C. Malingowski, Moosung Kim, Jue Liu, Liusuo Wu, Meigan C. Aronson, Peter G. Khalifah

Highlights

Graphical abstract

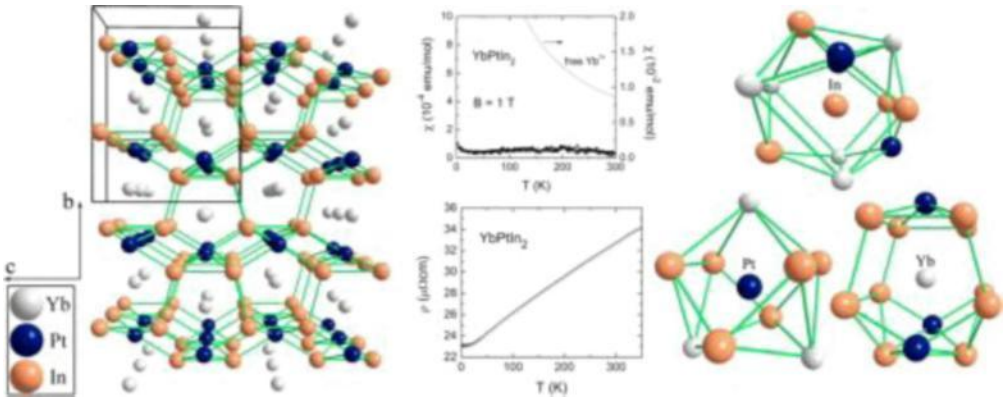

Highlights

► Flux growth method used to produce $Yb_{09}5PtIn_2$ single crystals. ► Found rare example of non-stoichiometry in a $MgCuAl_2$-type structure. ► The resistivity and diamagnetic response of $Yb0.9_5PtIn_2$ were modeled. ► DFT correctly predicts presence of Yb^{2+} in $Yb_{0.}9_5PtIn_2$. ► COHP results suggest other $MgCuAl_2$-type indides that may contain paramagnetic Yb^{3+}.

Structural and magnetic characterisation of the pyrochlores $Bi_{2-x}Fe_x(FeSb)O_7$, (x=0.1, 0.2, 0.3), $Nd1._8Fe_0.2(FeSb)O_7$ and $Pr_2(FeSb)O_7$

Original Research Article
Pages 316-322
Mariana J. Whitaker, Jose F. Marco, Frank J. Berry, Christina Raith, Elizabeth Blackburn, Colin Greaves

graphical abstract

Highlights

► The instability of the pyrochlore composition Bi_2FeSbO_7 is reported for the first time. ► Structure analysis confirms the presence of Fe on the Bi-site. ► The presence of Fe^{3+} on two distinct sites is supported by Mössbauer spectroscopy. ► For Nd_2FeSbO_7 and Pr_2FeSbO_7, Fe can also enter the Nd/Prsite. ► No magnetic order occurs in these materials.

Two proton-conductive hybrids based on 2,2′-biimidazole molecules and Keggin-type heteropolyacids

Original Research Article
Pages 323-329
Mei-Lin Wei, Jun-Hua Wang, Yu-Xia Wang

Highlights

► H_2biim shows the ability to form hydrogen bonds via the N-H groups in the context of crystal engineering. ► Heteropolyacids have suitable characteristics to be used excellent proton conductors. ► Two new supramolecular complexes based-on Keggin-type heteropolyacids and H_2biim molecules were constructed. ► The structure was determined by using single-crystal X-ray diffraction data. ► Both complexes showed good proton conductivities of 10^{-4} S cm^{-1} in the temperature range of 85-100°C.

Aluminium distribution in ZSM-5 revisited: The role of Al-Al interactions

Original Research Article
Pages 330-336
A. Rabdel Ruiz-Salvador, Ricardo Grau-Crespo, Aileen E. Gray, Dewi W. Lewis

Graphical abstract

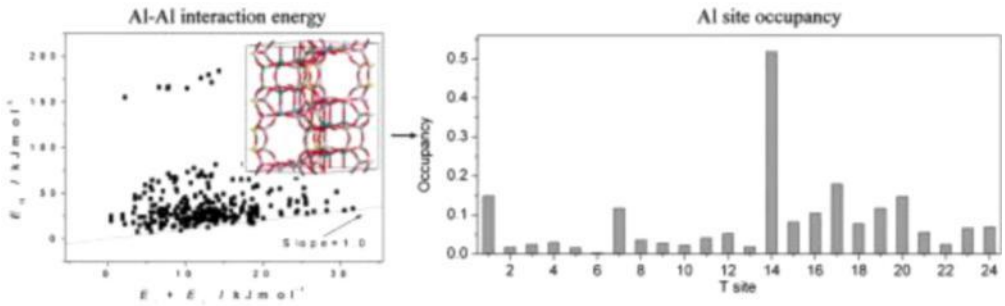

Highlights

► Si–Al distribution in ZSM-5 is revisited, stressing the role of the Al–Al interaction. ► Coulomb interactions are not the key factors controlling the Al siting. ► Anisotropy of the framework is identified as a source of departure from Dempsey's rule.

Electronic and optical properties of $TaO_{1-x}N_{1+x}$-based alloys

Original Research Article
Pages 337-343
Nabil Al-Aqtash, Florin Apostol, Wai-Ning Mei, Renat F. Sabirianov

Highlights

► The electronic and optical properties of TaON-based alloys are studied using DFT. ► The position of conduction and valence bands can be modified by varying N/O ratio. ► The band gap decreases monotonically with the increase of N/O ratio in $TaO1\text{-}_xN1_{+x}$. ► The band gap reduces in a series of fabricated alloys $ZrTa_3O_5N3 \rightarrow TaON \rightarrow YTa7O_7N_8$. ► The optical band gap decreases with the increase of N/O ratio.

Solid state phase equilibria and intermetallic compounds of the Al–Cr– Ho system

Original Research Article
Pages 344-356
Mingjun Pang, Yongzhong Zhan, Yong Du

Highlights

► Al-Cr-Ho system has been investigated. ► Al_9Cr_4 has cubic structure with space group *I43m.*

► Al_8Cr_4Ho crystallizes in $ThMn1_2$ type with space group *I*4/*mmm.* ► Al_4Cr phase is μ-type at 500 °C.

Measurement of host-to-activator transfer efficiency in nano-crystalline $Y_2O_3:Eu^{3+}$ under VUV excitation

Original Research Article
Pages 357-363
Christopher Waite, Rusty Mann, Anthony L. Diaz

Highlights

► We report on the optical properties of $Y_2O_3:Eu^{3+}$ prepared by combustion synthesis. ► Host-to-activator transfer efficiencies under VUV excitation were calculated. ► The low luminous efficiency of these materials is due to poor bulk crystallinity.

Indium hydroxide to oxide decomposition observed in one nanocrystal during in situ transmission electron microscopy studies

Original Research Article
Pages 364-370
Gerhard Miehe, Stefan Lauterbach, Hans-Joachim Kleebe, Aleksander Gurlo

Highlights

► In-situ time-resolved High Resolution Transmission Electron Microscopy. ► Crystallographic transformation path. ► Kinetics of the decomposition in one nanocrystal.

Well-ordered organic-inorganic hybrid layered manganese oxide nanocomposites with excellent decolorization performance

Original Research Article
Pages 371-378
Junli Zhou, Lin Yu, Ming Sun, Fei Ye, Bang Lan, Guiqiang Diao, Jun He

Highlights

► A two-step synthesis method was used to prepare the CTAB-Al-MO. ► The CTAB-Al-MO has the large basal spacing and high specific BET surface area. ► The thermal stability of the

well-ordered CTAB-Al-MO could obviously improve. ► The CTAB-Al-MO exhibits excellent oxidation and absorption ability to remove organic pollutants.

Synthesis, crystal structure, and vibrational spectroscopic and UV-visible studies of $Cs_2MnP_2O_7$

Original Research Article
Pages 379-385
Saida Kaoua, Saida Krimi, Stanislav Péchev, Pierre Gravereau, Jean-Pierre Chaminade, Michel Couzi, Abdelaziz El Jazouli

Graphical abstract

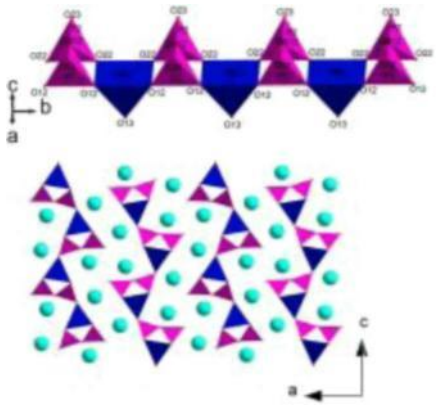

Highlights

► A new diphosphate, $Cs_2MnP_2O_7$, has been synthesized and structurally characterized. ► The structure consists of a 2D framework built up from (MnP_2O_7) sheets. ► The sheets consist of $[(MnO)P_2O_7]_\infty$ chains formed by P_2O_7 units and MnO_5 square pyramids. ► A factor group analysis leads to the determination of internal modes of (P_2O_7) groups. ► UV-visible spectrum consists bands assigned to d-d transitions of Mn^{2+} ion and to ODMn CT.

$Cu_2Mn1\text{-}_xCo_xSnS_4$: Novel këesterite type solid solutions

Original Research Article
Pages 386-391
F. López-Vergara, A. Galdámez, V. Manríquez, P. Barahona, O. Peña

Graphical abstract

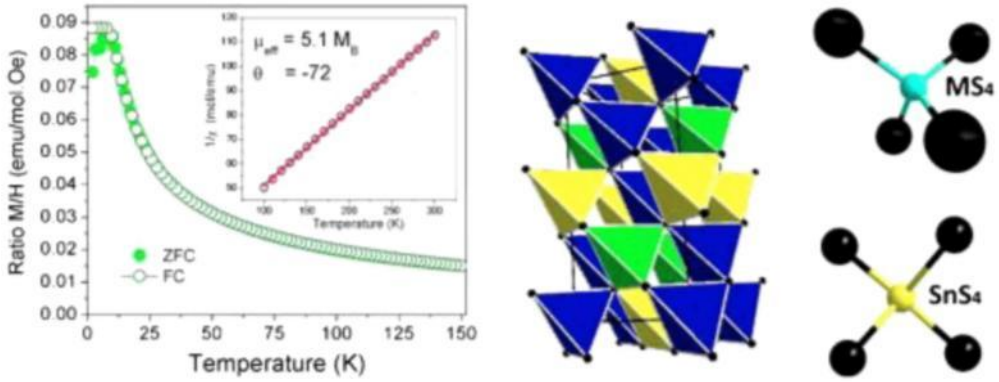

Highlights

► $Cu_2Mn_{1\text{-}x}Co_xSnS_4$ solid solutions belong to the family of compounds adamantine. ► Resolved single crystals of the solid solutions have space group ***ŭ***. ► The distortion of the tetrahedral volume of $Cu_2Mn_{1\text{-}x}Co_xSnS_4$ were calculated. ► These solid solutions are antiferromagnetic.

Particle and crystallite size effects on the modulated structure of multiferroic $CaMn_7O1_2$

Original Research Article
Pages 392-398
Wojciech Sławiński, Radosław Przeniosło, Izabela Sosnowska, Dariusz Wardecki, Andy N. Fitch, Mario Bieringer, Jacek B. Jasiński

Graphical abstract

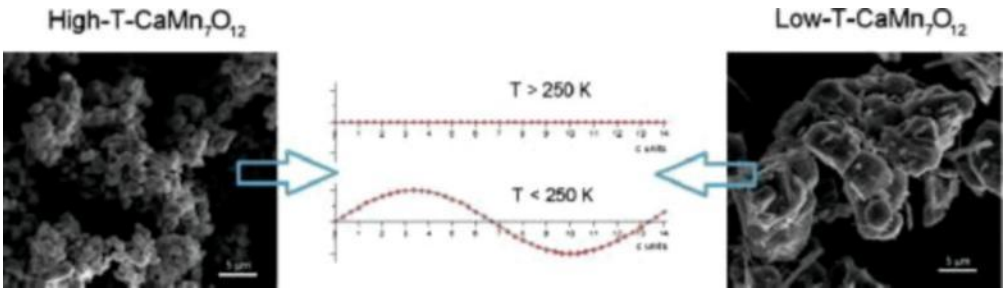

Highlights

► Atomic position modulation occurs in $CaMn_7O1_2$ with different particle sizes. ► The modulation length is the same for different $CaMn_7O1_2$ particle sizes. ► Nanowire shaped crystals of $CaMn_4O_8$ can be synthesized.

First-principles study of structural, electronic and thermodynamic properties of $EuMg_2$ and $EuMg_2H_6$

Original Research Article
Pages 399-406
Nan Bian, Zhou-Sheng Mo, Rong-Kai Pan, Ming-Hui Wang, Peng-Bo Li, Bi-Yu Tang

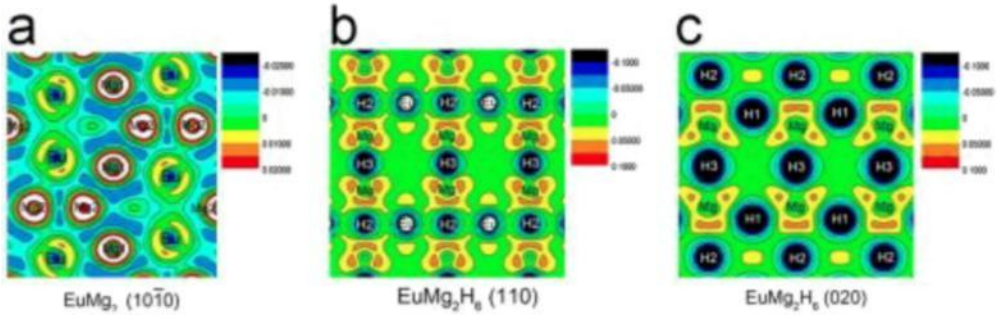

Highlights

► The Eu-*f* electron has important effects on stability and hydrogen storage behavior. ► The hydride exhibits primary ionic characteristics. ► Three types of MgDH bonding display also obvious ionic feature with some covalence. ► The dehydrogenation temperature of $EuMg_2H_6$ is further determined.

Local structures of $Sr_2FeMnO_{5+i;}$ 0=0, 0.5) and $Sr_2Fe1._5Cr_{0.5}O_5$ from reverse Monte Carlo modeling of pair distribution function data and implications for magnetic order

Original Research Article
Pages 407-415

Graham King, Farshid Ramezanipour, Anna Llobet, John E. Greedan

Graphical abstract

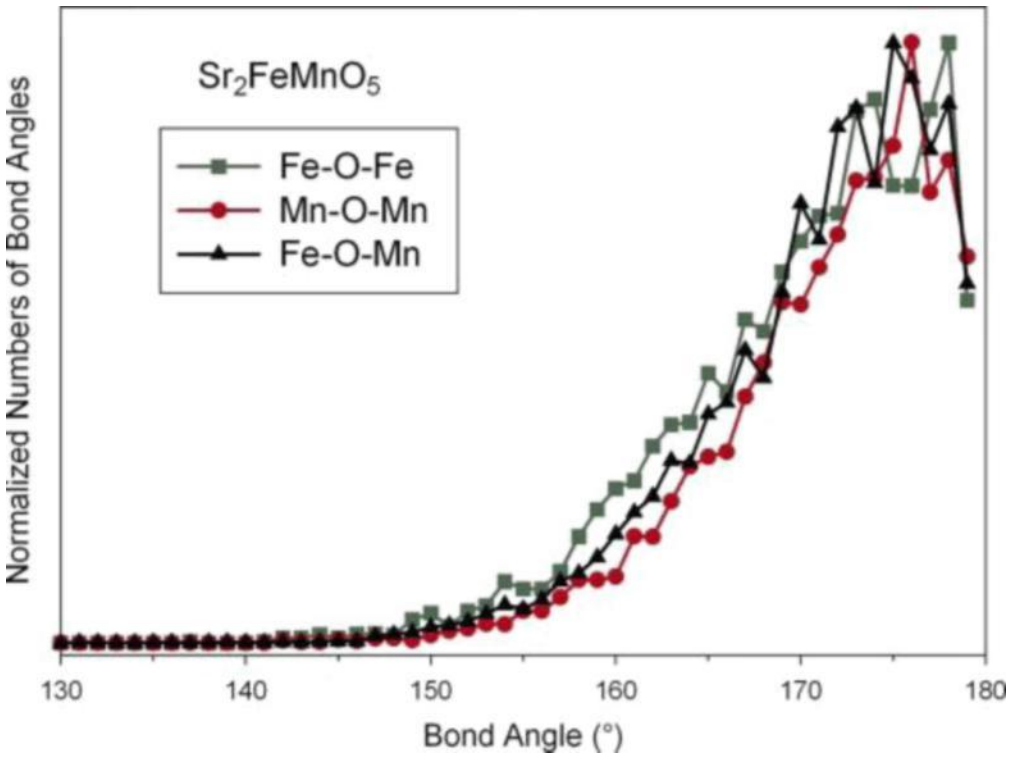

Highlights

► No long range ordering of oxygen vacancies, but short range order is present. ► No short range Fe/Mn order but short range Fe/Cr order is present. ► Fe tends to have lower coordination numbers while Mn and Cr have higher ones. ► Local bond distances and bond angles have been determined. ► Local structures can help explain long range magnetic ordering behavior.

Hydrothermal syntheses, crystal structures and luminescence properties of zinc(II) and cadmium(II) coordination polymers based on bifunctional 3,2′:6′,3″-terpyridine-4′-carboxylic acid

Original Research Article
Pages 416-423
Na Li, Hui-Lin Guo, Huai-Ming Hu, Juan Song, Bing Xu, Meng-Lin Yang, Fa-Xin Dong, Gang-Lin Xue

Highlights

► Five new zinc/cadmium metal-organic frameworks have been hydrothermal synthesized. ►

The structural variation is attributed to the diverse metal ions and auxiliary ligand. ► Compounds 1-5 exhibit 1D ring chain, 2D layer and 3D open-framework, respectively. ► These compounds exhibit strong solid state luminescence emission at room temperature.

Metal arsonate polymers of Cd, Zn, Ag and Pb supported by 4-aminophenylarsonic acid

Original Research Article
Pages 424-432
Leslie A. Lesikar-Parrish, Robert H. Neilson, Anne F. Richards

Highlights

► The synthesis of five novel metal arsonates with 4-aminophenyl arsonic acid. ► Single crystal X-ray diffraction studies revealed polymeric structures. ► The luminescent properties of the metal arsonates were investigated.

Structural, electronic and thermodynamic properties of R_3ZnH_5 (R=K, Rb, Cs): A first-principle calculation

Original Research Article
Pages 433-439
Jia Li, Shengli Zhang, Shiping Huang, Peng Wang, Huiping Tian

Graphical abstract

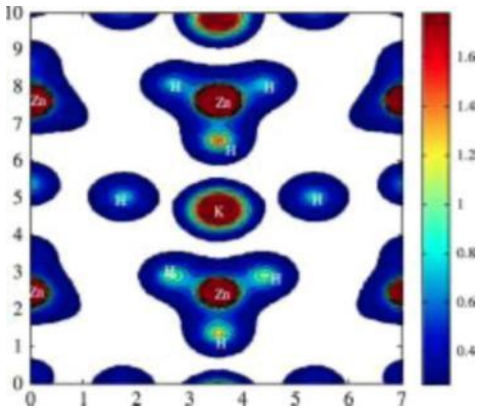

Highlights

► Electronic and thermodynamic properties of R_3ZnH_5 (R=K, Rb, Cs) were calculated. ► The formations of R_3ZnH_5 hydrides are all exothermic at 298 K. ► The thermodynamic stabilities

decrease with the increasing diameter of R atom. ► Two possible decomposition pathways of R_3ZnH_5 were investigated.

An unusual 3D interdigitated architecture assembled from Keggin polyoxometalates and dinuclear copper(II) complexes

Original Research Article
Pages 440-444
Haijun Pang, Ming Yang, Lu Kang, Huiyuan Ma, Bo Liu, Shaobin Li, Heng Liu

Highlights

► The first example of interdigitated architecture assembled by POMs and dinuclear copper(II) complexes is observed. ► A zipper-like pattern is observed in the structure. ► The IR, TG, XRPD, magnetism and electrochemical property of the title compound were studied.

High pressure synthesis and crystal structure of a ternary superconductor $Ca_2Al_3Si_4$ containing layer structured calcium sub-network isomorphous with black phosphorus

Original Research Article
Pages 445-451
Masashi Tanaka, Shuai Zhang, Yuki Tanaka, Kei Inumaru, Shoji Yamanaka

Highlights

► A typical Zintl compound $CaAl_2Si_2$ melts congruently at ambient pressure. ► Under high pressure $CaAl_2Si_2$ decomposes to $Ca_2Al_3Si_4$ and Al at ~600 °C. ► $Ca_2Al_3Si_4$ contains Ca sub-network isomorphous with black phosphorus. ► $Ca_2Al_3Si_4$ shows superconductivity with a transition temperature of 6.4 K.

Preparation and optical characteristics of layered perovskite-type lead-bromide-incorporated azobenzene chromophores

Original Research Article
Pages 452-458
Ryo Sasai, Hisashi Shinomura

Graphical abstract

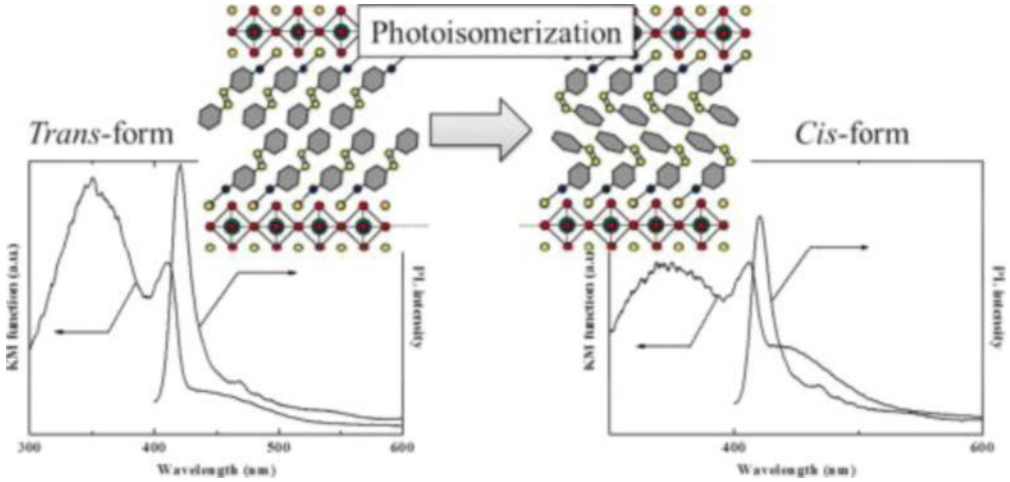

Highlights

► PbBr-based layered perovskite with azobenezene derivatives could be synthesized by a homogeneous precipitation method. ► Azobenzene derivatives incorporated the present hybrid that exhibited reversible photoisomerization under UV and/or visible light irradiation. ► PL property of the present hybrid could also be varied by photoisomerization.

Enhanced performance of dye-sensitized solar cells based on TiO_2 with NIR-absorption and visible upconversion luminescence

Original Research Article
Pages 459-465
Li Liang, Yang Yulin, Zhou Mi, Fan Ruiqing, Qiu LeLe, Wang Xin, Zhang Lingyun, Zhou Xuesong, He Jianglong

Graphical abstract

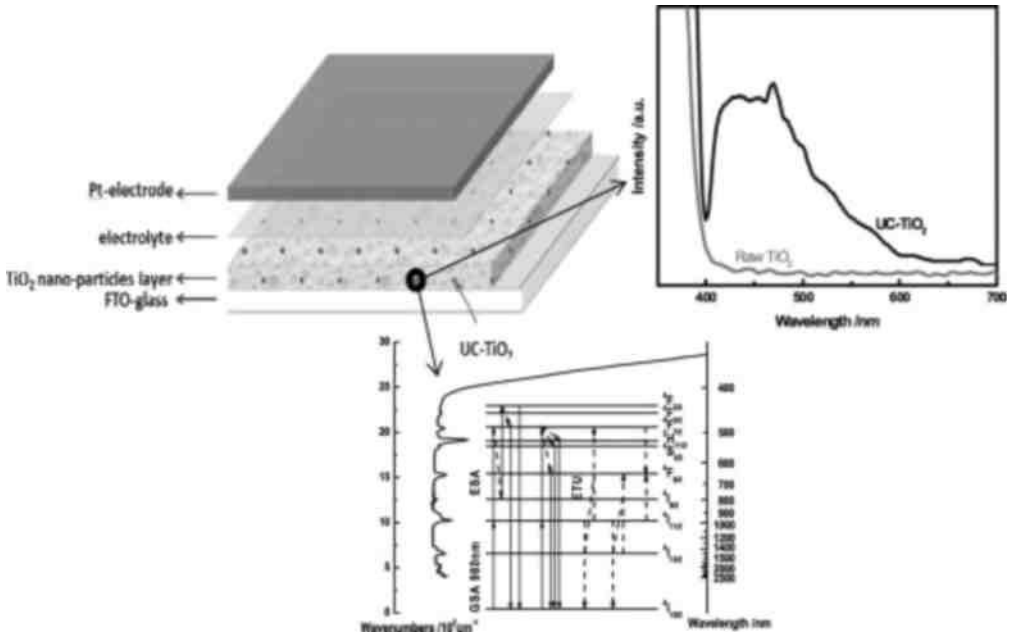

Highlights

► TiO_2 with NIR-absorption and visible up-conversion luminescence (UC-TiO_2) was prepared by a sol-gel method. ► A systematic characterization and analysis was carried out to discuss the mechanism. ► A significantly enhanced performance of DSSC was explored by using UC-TiO_2 as an additive.

Towards new binary compounds: Synthesis of amorphous phosphorus carbide by pulsed laser deposition

Original Research Article
Pages 466-474
Judy N. Hart, Paul W. May, Neil L. Allan, Keith R. Hallam, Frederik Claeyssens, Gareth M. Fuge, Michelle Ruda, Peter J. Heard

Graphical abstract

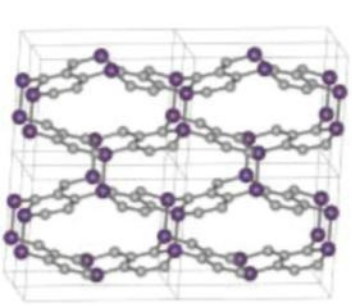

Predicted structure for PC_3

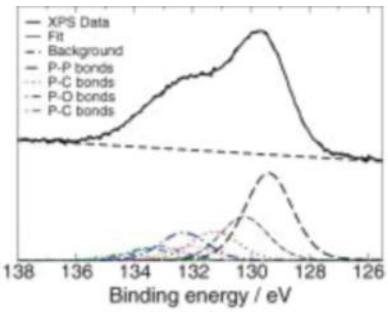

Phosphorus 2*p* XPS peak including P-C bonding environments consistent with predictions

Highlights

► We have synthesised amorphous phosphorus–carbon films by pulsed laser deposition. ► X-ray photoelectron spectroscopy results indicate formation of direct P–C bonds and hence phosphorus carbide. ► Local bonding environments are consistent with those in predicted structures.

Electronic and structural influence of Ni by Pd substitution on the hydrogenation properties of TiNi

Original Research Article
Pages 475-484
Hoda Emami, Raphaël Souques, Jean-Claude Crivello, Fermín Cuevas

Graphical abstract

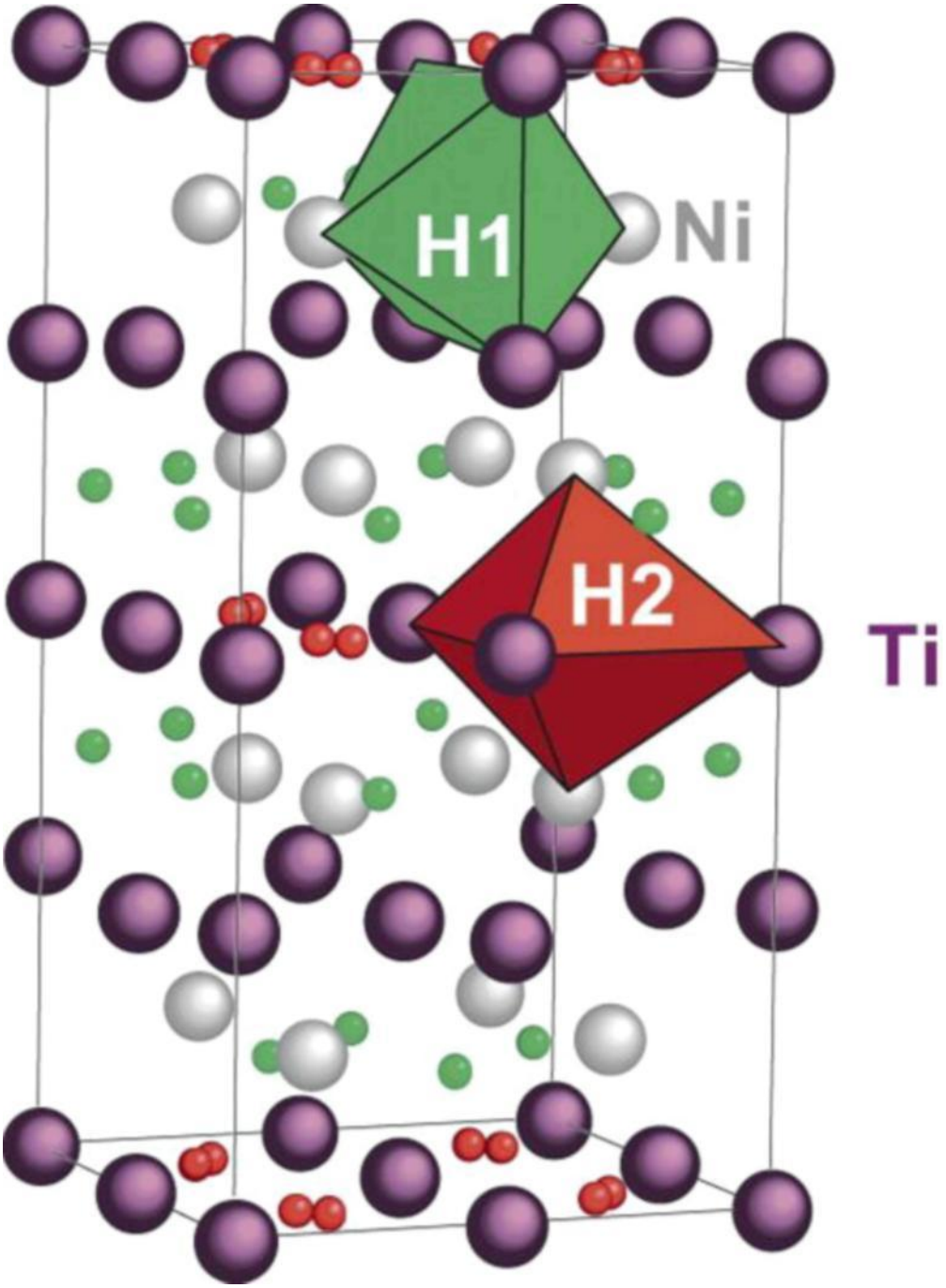

Highlights

► Neutron Diffraction and DFT calculations have been done on $TiNi_{1-x}Pd_xH_y$ compounds. ► Electronic effect of Pd substitution governs the hydrogenation properties in TiNi. ► The rule of reverse stability in intermetallics/hydrides is observed with Pd substitution. ► The hydrogen atoms in the *I*4/*mmm* structure prefer to occupy the 16*n* site.

Reverse micelles directed synthesis of TiO_2–CeO_2 mixed oxides and

investigation of their crystal structure and morphology

Original Research Article
Pages 485-495
Lenka Matějová, Václav Valeš, Radek Fajgar, Zdeněk Matěj, Václav Holý, Olga Šolcová

Graphical abstract

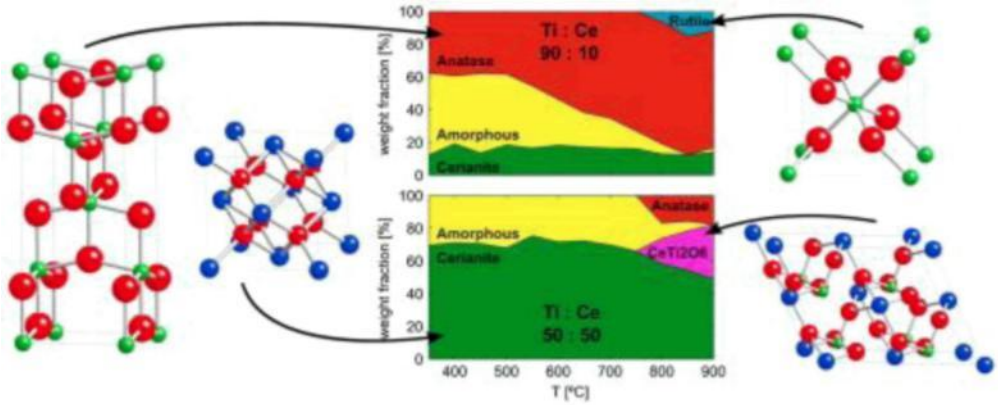

Highlights

► Ti/Ce oxides were prepared using reverse micelles of Triton X-114. ► Crystallization of TiO_2, CeO_2 or $CeTi_2O_6$ depends on Ti:Ce molar ratio. ► Amorphous phase attributed to TiO_2 was identified. ► Metal oxides surface area is influenced by the character of present carbon impurities.

pH control of the structure, composition, and catalytic activity of sulfated zirconia

Original Research Article
Pages 496-505
Vladimir K. Ivanov, Alexander Ye. Baranchikov, Gennady P. Kopitsa, Sergey A. Lermontov, Lyudmila L. Yurkova, Nadezhda N. Gubanova, Olga S. Ivanova, Anatoly S. Lermontov, Marina N. Rumyantseva, Larisa P. Vasilyeva, Melissa Sharp, P. Klaus Pranzas, Yuri D. Tretyakov

Graphical abstract

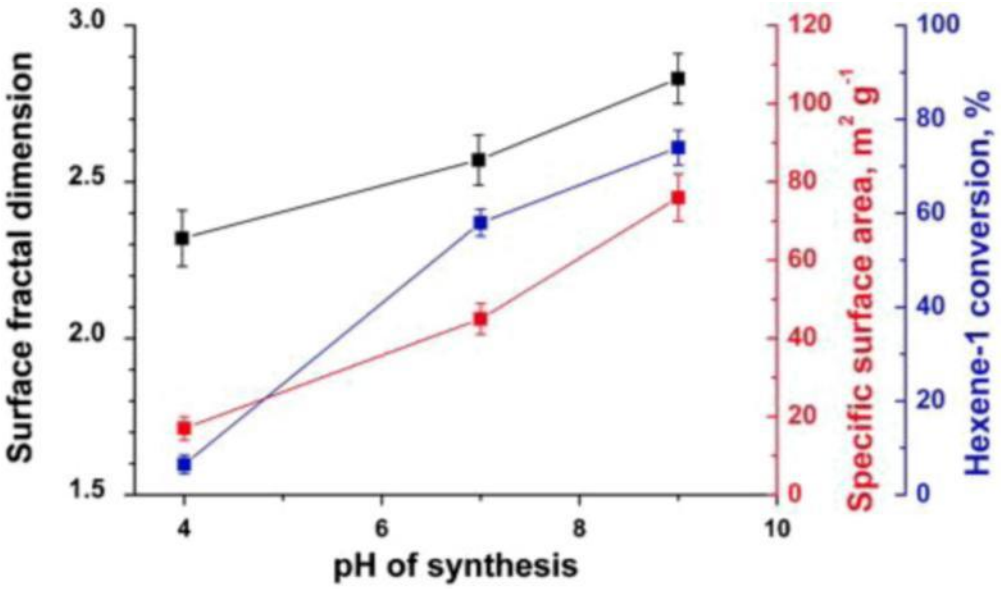

Highlights

► Structural transformation of amorphous hydrous zirconia into sulfated zirconia is studied. ► Precipitation pH controls surface fractal dimension of amorphous zirconia gels. ► Precipitation pH is the key factor governing properties of sulfated zirconia.

$Fe(CN)_6^{3-}/Fe(CN)_6^{4-}$ redox in the interlayer determined by the charge density of Zn_nCr-layered double hydroxides

Original Research Article
Pages 506-510
Jia Zhang, Yunfeng Xu, Jiangyong Liu, Jizhi Zhou, Zhi Ping Xu, Guangren Qian

Graphical abstract

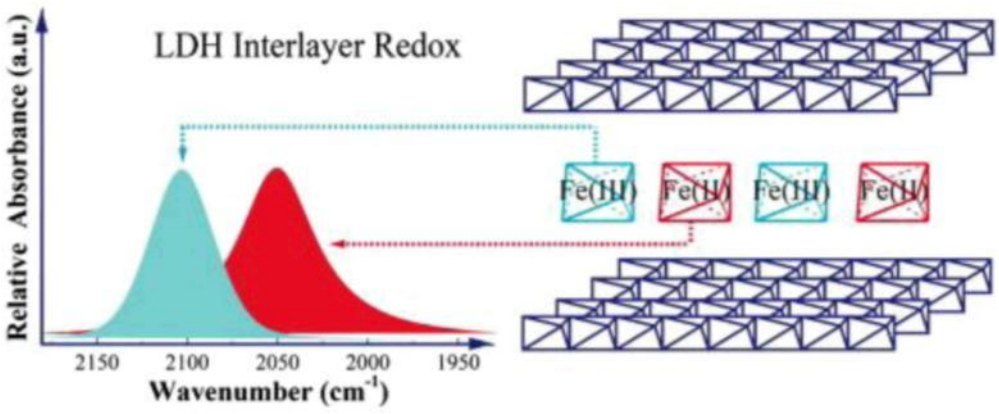

Highlights

► An interlayer redox phenomena was observed in $Fe(CN)_6^{3/4}$- intercalated ZnCr-LDHs. ► The ratio of interlayer redox was examined by FTIR fitting analysis. ► The tendency of redox was influenced by Zn:Cr molar ratio. ► The mechanism relies on the charge density of metal hydroxyl layer.

A comparative study of optical absorption and photocatalytic properties of nanocrystalline single-phase anatase and rutile TiO_2 doped with transition metal cations

Original Research Article
Pages 511-519
L. Kernazhitsky, V. Shymanovska, T. Gavrilko, V. Naumov, V. Kshnyakin, T. Khalyavka

Graphical abstract

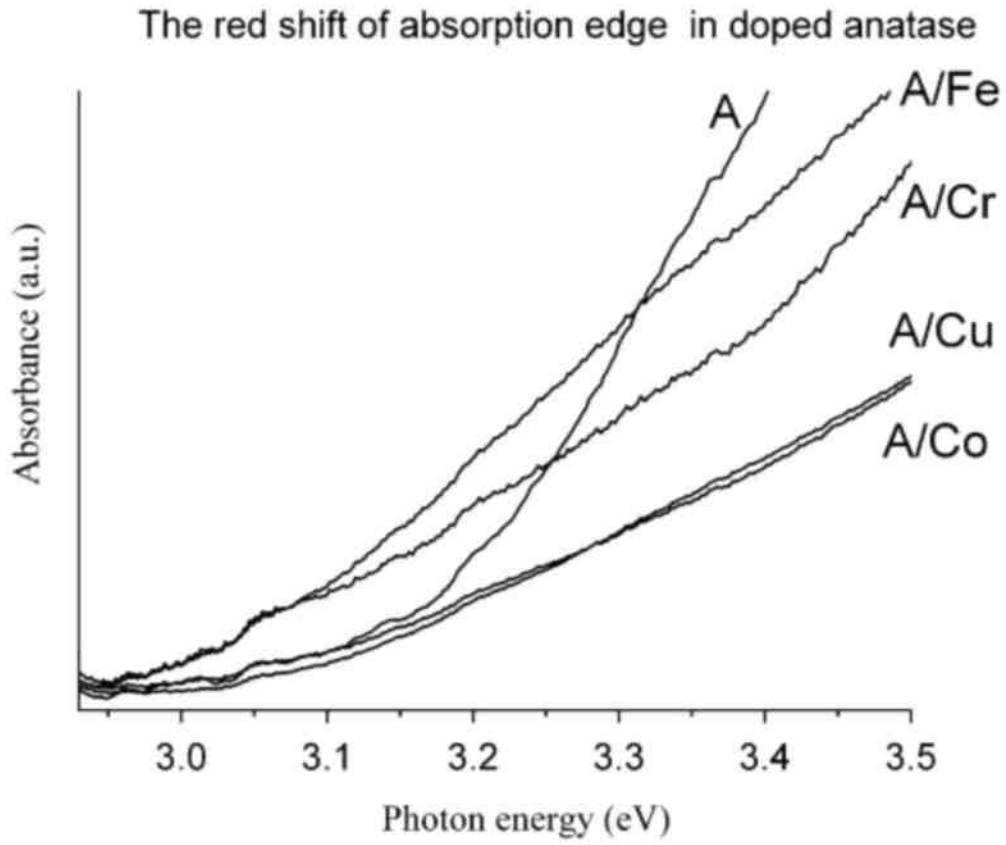

Highlights

► Single-phase anatase and rutile powders surface-doped with transition metal cations. ► Absorption edge and band gap of rutile do not change with surface doping. ► Band gap of

surface-doped anatase reduces being the lowest for *A/Fe*. ► The surface-doping improves photocatalytic activity of anatase. ► The surface-doping inhibits photocatalytic activity of rutile.

High-pressure synthesis, crystal structure and magnetic property of ilmenite-type $FeGeO_3$

Original Research Article
Pages 520-524
Daisuke Nakatsuka, Takashi Yoshino, Jun Kano, Hideki Hashimoto, Makoto Nakanishi, Jun Takada, Tatsuo Fujii

Graphical abstract

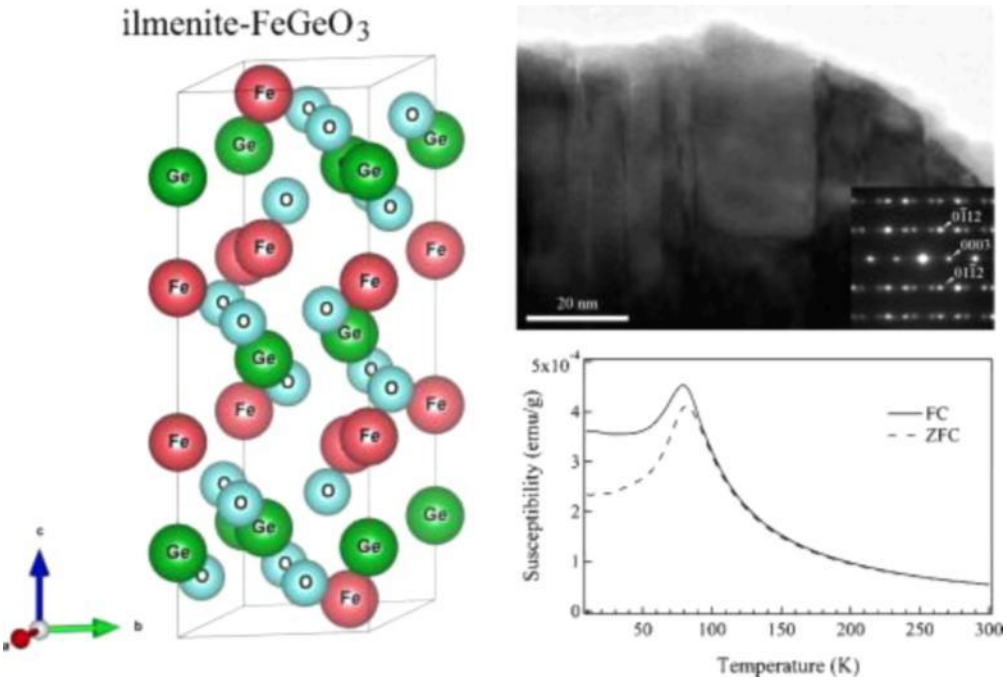

Highlights

► Ilmenite-type $FeGeO_3$, a novel polymorphism of $FeGeO_3$ was successfully synthesized. ► It was synthesized by using high pressure technique at 23.5 GPa at 500 °C. ► Subsequent annealing in vacuum was effective to improve the crystallinity. ► Its primary particle size was ~15 nm, and some grains had lamellar microstructure. ► It showed typical antiferromagnetic behavior with the Néel temperature of 79 K.

High-temperature order-disorder transitions in the skutterudites $CoGe_{1.5}g_{1.5}$ (g=S, Te)

Original Research Article
Pages 525-531

Andreas Kaltzoglou, Anthony V. Powell, Kevin S. Knight, Paz Vaqueiro

Graphical abstract

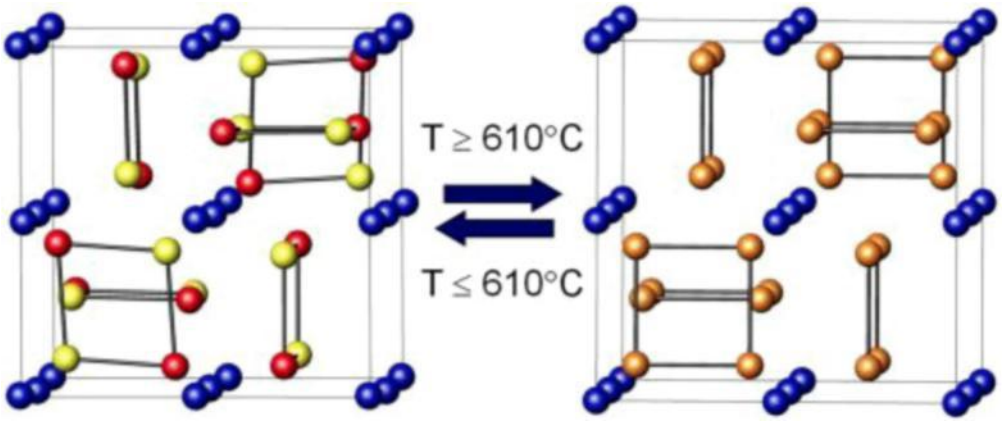

Highlights

► CoGe1.5S1.5 retains an ordered skutterudite structure up to 950 °C. ► $CoGe1.5Te1.5$ undergoes an order-disorder phase transition at 610 °C. ► Below 610 °C, anions are arranged *trans* to each other within Ge_2Te_2 rings. ► Above 610 °C, anions are statistically distributed within the Ge_2Te_2 rings. ► The effect of the phase transition on the thermal conductivity is discussed.

Incommensurate structure of $GdBaCo_2O_{5+(5}$ *(tf~0.38)*

Original Research Article
Pages 532-541
N. Ishizawa, T. Asaka, T. Kudo, K. Fukuda, N. Abe, T. Arima

Graphical abstract

Highlights

► The oxygen deficient $GdBaCo_2O_{5+f5}$ has an incommensurate five-dimensional structure. ► The modulation vectors are close to 1/3 of *a* □ of a tetragonal fundamental unit cell. ► The magnitude of the modulation vectors increased upon heating the crystal. ► The typical structure contains square-pyramidal CoO_5 arrays intersecting with each other. ► The O atom deficiency in the GdO plane causes positional modulations of all atoms.

Synthesis of nanostructured AlN by solid state reaction of Al and diaminomaleonitrile

Original Research Article
Pages 542-547
S.A. Rounaghi, H. Eshghi, A.R. Kiani Rashid, J. Vahdati Khaki, M. Samadi Khoshkhoo, S. Scudino, J. Eckert

Graphical abstract

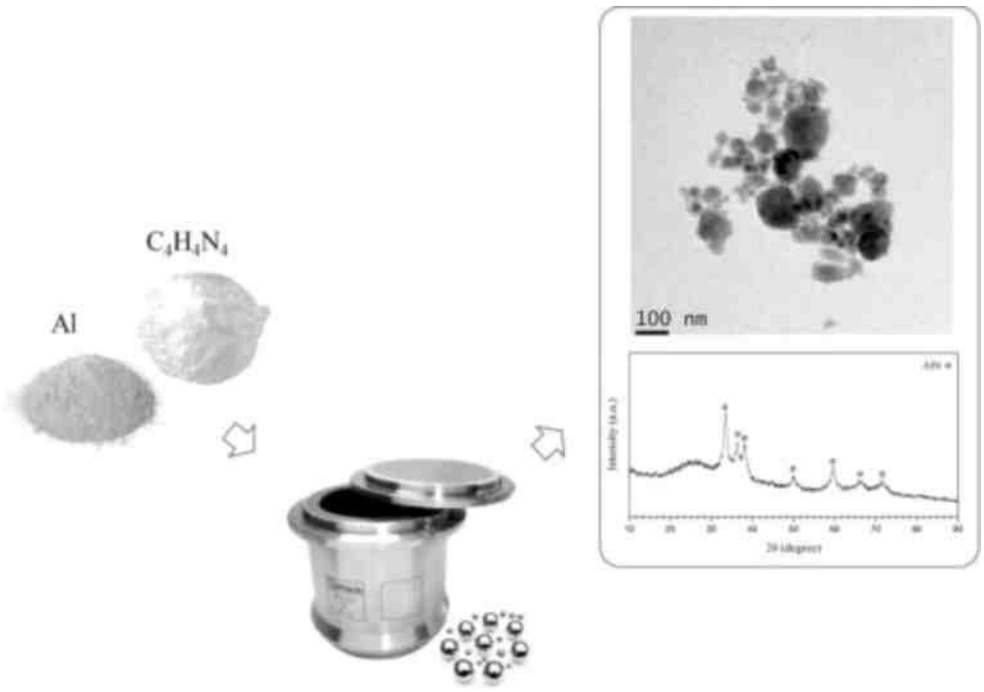

Highlights

► Solid state reaction of diaminomaleonitrile (DAMN) with Al was studied via mechanochemical and thermal treatment routs. ► Nanocrystalline AlN was successfully synthesized by the mechanochemical process. ► The C/N material was formed by

polymerization of DAMN during the thermal treatment process. ► No reaction between DAMN and Al was detected during the thermal treatment method.

Corrigendum

Corrigendum to “Structure and high temperature thermoelectric properties of $SrAl_2Si_2$” [J. Solid State Chem. 182 (2009) 240–245]

Page 149
Susan M. Kauzlarich, Cathie L. Condron, Jonathan K. Wassei, Teruyuki Ikeda, G. Jeffrey Snyder

Corrigendum to “High magnetic ordering temperature in the perovskites $Sr_{4-x}La_xFe_3ReO_{12}$ (x=0.0, 1.0, 2.0)” [J. Solid State Chem. 194 (2012) 48–58]

Page 246
M. Retuerto, M.-R. Li, Y.B. Go, A. Ignatov, M. Croft, K.V. Ramanujachary, R.H. Herber, I. Nowik, J.P. Hodges, W. Dachraoui, J. Hadermann, M. Greenblatt